PCCP

Accepted Manuscript

ROYAL SOCIETY OF CHEMISTRY

www.rsc.org/pccp

Growth mechanisms of Pd nanofilms electrodeposited onto Au(111): an *in situ* grazing incidence X-ray diffraction study

Yvonne Soldo-Olivier[1,2,3], M. De Santis[3] , W. Liang[1,2] and E. Sibert[1,2]

[1]Univ. Grenoble Alpes, LEPMI, F-38000 Grenoble, France

[2]CNRS, LEPMI, F-38000 Grenoble, France

[3] CNRS, Institut Néel, F-38042 Grenoble, France

Corresponding author yvonne.soldo@neel.cnrs.fr

Abstract

Ultra-thin Pd films electrochemical deposition onto Au(111) single crystal in a chloride containing solution was studied with *in situ* Surface X-Ray Diffraction measurements. We report the detailed description of the growth mode, as well as the film morphology and the lattice parameters as a function of the thickness, from 2 up to 10 monolayers (ML) as equivalent thickness.

An almost ideal layer-by-layer pseudomorphic growth is observed up to two deposited ML. For higher thicknesses, it is followed by the growth of large 3D Pd bulk like islands. They are about 20±5 ML high and ~220 Å as diameter for the Pd_{4ML} film and occupy only about 20% of the surface. Their height increases faster than their size with the Pd deposited amount.

We could clearly show that chlorides do not play any role in inhibiting the three dimensional growth of Pd/Au(111) films. We could also unequivocally correlate the features observed by electrochemical surface characterisation in acidic medium with the detailed structure obtained by diffraction.

Keywords: Pd nanofilms, in situ surface diffraction, electrochemical deposition, epitaxial growth

1. Introduction

The interest in ultra-thin metallic over-layers has grown in various fields of physical chemistry and numerous are their industrial applications. Detailed information on the growth and the

structure of the supported layers are necessary for both scientific and technological reasons. Several studies have been dedicated to the ultra-thin film electro-deposition onto well-ordered single crystals like Pt, Au, Cu,… [1, 2].

Compared to the physical techniques (molecular beam epitaxy, sputtering…), the electrochemical way is relatively straightforward, less expensive and allows to obtain in a reproducible and controlled way single-crystal metallic deposits of very good quality.

Pd/Au(111) represents a very interesting model system for the study of various electrochemical reactions like formic acid and formaldehyde oxidation [3, 4], CO electro-oxidation [5, 6], oxygen reduction [7] or hydrogen storage processes [8, 9].

Pd electrodeposition onto Au(111) in acidic media is characterised by the presence of the UnderPotential Deposition (UPD) phenomenon. This first atomic layer deposition, which occurs at a potential value higher than the Nernst potential, was observed with palladium sulphate [10], palladium nitrate and palladium perchlorate [11].

The pseudomorphic character of the first Pd UPD layer electrodeposited in solution containing tetrachloropalladate was shown with *in situ* Scanning Tunnelling Microscopy (STM) images [12] and Surface X-Ray Diffraction (SXRD) [13].

Structure of the thicker layers remains controversial, in particular concerning the role of anions in the deposition solution. Using *in situ* STM images, Köntje *et al.* [11] observe that Pd growth is two dimensional up to almost two Pd layers, regardless of the anion (chloride, sulphate, nitrate or perchlorate) in the solution. With the same technique, Kibler *et al.* [12] in 0.1 M H_2SO_4+0.1mM H_2PdCl_4 have shown a pseudomorphic growth of Pd up to four layers, with a Moiré pattern observed on the fifth layer. Nevertheless, attempts to resolve the Pd atomic structure failed, because of the presence of a hexagonal Pd chloro complex adlayer. First and second layers grow flat, while the dendritic third layer starts to nucleate before the second layer has been completed. No surface alloy with Au(111) is revealed, in opposite to findings in UHV studies [14].

By contrast, *in situ* SXRD experiments in a 0.1 M H_2SO_4 + 1 mM K_2PdCl_4 electrolytic solution [13, 17] do not observe the pseudomorphic layer-by-layer growth up to two Pd layers: the non-specular profiles indicate that the second and the third layer are relaxed. Interplanar distances between the Pd bulk like layers are surprisingly small, in particular that between the third and fourth Pd layer equal to 2.08 Å.

Naohara *et al.* [15,16] made *in situ* STM and electrochemical quartz crystal microbalance experiments supporting the model that $PdCl_4^{2-}$ complex plays an important role to inhibit the three-dimensional growth. Similar conclusions are given by Tang *et al. in situ* STM

measurements [10], showing that Pd deposited from chloride-free solution presents a higher tendency for three-dimensional growth than deposited from chloride-containing solution. In detail, they observe a pronounced three-dimensional growth of Pd on top of the second monolayer, Pd forming tremendously huge deposits at stepped sites for higher coverage than two layers, while first and second layer are pseudomorphic. They say that, at comparable coverages, the properties of the pseudomorphic Pd layer are more pronounced for deposition from sulphate solution.

To achieve a better inside into the role of anions in the Pd/Au(111) growth, we recently studied the growth of the first Pd layers electrochemically deposited onto Au(111) in a sulfuric acidic solution with tetrachloropalladate and extra chloride [18]. Measuring with *in situ* SXRD the anti-Bragg (0,1,0.5) reflection, we found that the two first layers are pseudomorphic, following the fcc close packed stacking of the substrate. The third layer growth begins before the second one completion and the following layers are relaxed. Nevertheless, a detailed description of the Pd ultra-thin films structure could not be achieved due to the lack of a full set of crystal truncation rods (CTRs) measurements. Electrochemical characterisation seemed to indicate the presence of huge 3D Pd islands leaving large parts of the second Pd layer uncovered, quite flat on their top, but no detailed structural characterisation could support this model.

In order to clarify the controversial structure of the first Pd adlayers electrochemically deposited in presence of chloride onto Au(111), this paper presents detailed *in situ* SXRD measurements on Pd ultrathin films from 2 ML up to about 10 ML as equivalent thickness. This surface structural characterization at the atomic level allows giving a better insight into the role of chloride in the Pd/Au(111) growth mechanisms and validating unequivocally the use of electrochemistry to get the detailed surface characterisation of this system.

2. Methods

Pd electrochemical deposition

Prior to Pd deposition, Au(111) single crystal (10 mm diameter, MaTecK Jülich, Germany, miscut less than 0.1°) was flame annealed (butane/air) and cooled down in air. The quality and the cleanliness of the surface were checked by cyclic voltammetry in 0.1 M H_2SO_4 [19]. A Saturated Calomel Electrode (SCE) was used as reference electrode. In the following, all potentials are expressed *versus* Reversible Hydrogen Electrode (RHE) potential (0 V *vs.* SCE =

+0.298 V *vs.* RHE in 0.1 M H_2SO_4). The working electrode was polarized before being put in contact with electrolyte and potential was maintained until breakup of the contact. Electrode was always transferred between cells with a protective water droplet in order to minimize surface contamination.

Gold is the only fcc metal that exhibits a reconstruction of the close packed (111) surface [20, 21], presenting a different atomic arrangement from cleaved-bulk configuration. This herringbone surface reconstruction, also referred to as striped phase, results from the spontaneous formation of stress domains. It corresponds to an uniaxial surface dislocation network typically referred to as $(p \times \sqrt{3})$ structure, where $p \approx 22$, and is characterized by an average contraction of the reconstructed Au surface layer of 4.5%.

Au(111) surface in electrochemical environment is unreconstructed at potentials more positive than a critical (electrolyte-dependent) potential, whereas herringbone surface reconstruction is formed at more negative potentials [22, 23]. Theoretical studies suggest that this potential induced phase transition is due to the adsorption of anions [24].

Figure 1 shows the characterization of a crystal with a relatively high surface quality. The anodic peak 1 around 0.596 V *vs.* RHE is assigned to the transition from the reconstructed $\sqrt{3}$ ×22 phase at lower potential to the (1×1) surface at higher potential; the corresponding peak 1' shows the reverse process. The anodic spike 2 at 1.096 V *vs.* RHE is associated to the adsorbed sulphate phase transition from disordered to $(\sqrt{3} \times \sqrt{7})$ R19.1° ordered structure. Anodic 1 and 2 peaks are particularly sensitive to the presence of defects on the Au(111) surface, so they can be used as indicators for the quality of the electrode's surface [19].

In our experimental conditions Au(111) surface is in the unreconstructed (1x1) phase, as the herringbones reconstruction in acidic electrochemical environment is typically formed at lower potential values than those involved during Pd electro-deposition, as detailed in the next paragraph.

Pd electrochemical deposition was made in a 0.1 M H_2SO_4 + 0.1 mM $PdCl_2$ + 3 mM HCl solution using a Biologic VSP potentiostat. The Au(111) electrode was introduced at 0.998 V *vs*. RHE; potential was then negatively scanned at 0.1 $mV.s^{-1}$ down to 0.76 V *vs.* RHE in the Pd bulk deposition region and maintained at this value until the equivalent deposition of the desired thickness was obtained. The amount of deposited Pd was monitored through the coulometric charge, assuming one palladium atom for each surface gold atom and a two-electron charge transfer. In the following discussion, the Pd deposit will be referred to as Pd_{xML}/Au(111). After

deposition, the crystal was transferred under Ar atmosphere into the thin layer electrochemical cell dedicated to the SXRD experiments. Prior to diffraction experiments, surface cleanness was checked by cyclic voltammetry in this cell [18].

In situ SXRD experiments

Data were collected using the five-circle diffractometer on the D2AM French CRG beamline at the European Synchrotron Radiation Facility (ESRF, France), with a monochromatic incident beam of 23.5 keV. A unit cell was chosen to index the reflections with A_1 and A_2 defining a hexagonal mesh in the surface plane. A_3 is perpendicular to the surface and its length equals the period of the fcc close packing stacking: $A_1=(a_{Au}/2)*[1\text{-}10]$, $A_2=(a_{Au}/2)*[01\text{-}1]$, and $A_3=a_{Au*}[111]$, a_{Au} being the bulk lattice constant of gold .

Three different equivalent thicknesses for the Pd films have been investigated: Pd_{2ML}/Au(111), Pd_{4ML}/Au(111) and Pd_{10ML}/Au(111). Several samples were measured for the intermediate thickness.

A dedicated thin layer electrochemical cell for *in situ* SXRD experiments was used, described elsewhere [25, 26]. Diffracted signal was recorded under potential control (PAR 273A Potentiostat) at 0.198 V *vs*. RHE, in 0.1 M H_2SO_4. (10), (01) and (11) Crystal Truncation Rods (CTRs) [27] and the equivalent (-12) and (-11) reflections were measured in grazing incidence (1°) integrating the signal collected while rocking the crystal around its surface normal at several L values in between the Bragg peaks. Indeed, diffracted intensities far from the Bragg peaks are sensitive to the structure of the surface. In the following, (01) CTR will be plotted as the negative L range of the (10) CTR, (01L) reflections being equivalent to (10-L) ones due to crystal symmetry. Specular reflectivity [(00) CTR] and other specific reciprocal space line scans were also measured. The structure factor moduli were extracted from the integrated intensity by applying standard correction factors [28] adapted to the diffractometer geometry and by considering water absorption effect. Error bars for the structure factors are based on the agreement factor between equivalent reflections [29]. Data analysis was performed with the ROD package [30]. The structural parameters were optimized through a fit of the structure factors, employing a χ^2 minimization for the refinement.

3. Results and discussion

3.1 Structure of the ultra-thin adlayers: Pd_{2ML}/Au(111)

Experimental CTR for the Pd_{2ML}/Au(111) deposit are reported in figure 2. The specular CTR (Fig. 2a) shows a bump in the middle between the direct beam and the first Bragg peak positions, which qualitatively characterizes a 2 ML thick deposit. This same feature is observed on the non-specular CTRs, as expected for a pseudomorphic growth. A model was taken for the surface structure with Pd atoms occupying fcc sites in coherent continuation with the substrate. The occupancy of the first Pd deposited layer τ_1 was set equal to one, since the electrochemical characterization of the electrode did not reveal the presence of even partially free Au(111) surface, which would result in the characteristic 1/1' and 2/2' peaks (see figure 1) [18].

The second layer occupancy was left free and the best fit is reached with an occupation rate τ_2 of about 2/3. In first simulations, we considered the possibility of Pd diffusion into first Au layers: we concluded that, if any, it is below a few percent of one monolayer.

The vertical displacement of the Pd atomic layers as well as of the Au layer at the interface was optimised. The interplanar distance between the two last gold layers (2.328±0.004 Å) is slightly smaller than for bulk Au (2.3545 Å). Au-Pd interface distance is equal to 2.275±0.015 Å. The interlayer distance between the two Pd layers ($d_{Pd1\text{-}Pd2}$ =2.20±0.03 Å) is smaller than the corresponding Pd bulk one ($d_{Pd\ (111)}$=2.246 Å). Indeed, due to the mismatch between Pd and Au bulk lattice, the deposited Pd_{2ML}/Au(111) film is strained. The pseudomorphic growth implies an in plane expansion of the atomic distances of about 4.8%, which is accompanied by a compression of the interplanar distance by about 2% compared to bulk Pd.

It was observed that the tensile stress of metallic overlayers on metal surfaces can be relieved by partial dislocations inducing the presence of hcp sites [31]. In order to check for the presence of such dislocations in the film, a modelling was made including the possibility of hcp sites. The best fit gives 6% of hcp site at the interface, with the second layer following an fcc stacking with respect to the first Pd and the interface Au layers. This doesn't improve the fit quality yielding the same χ^2. Even if the presence of partial dislocations cannot therefore be excluded, it would concern only a small fraction of the first Pd layer.

Debye Waller parameter was also optimized for Pd atoms. The larger "in-plane" value (15±1 $Å^2$), compared to the "out-of-plane" one (0.44 ±0.25 $Å^2$), reflects the higher disorder in this direction. This can be qualitatively understood reminding that the pseudomorphic Pd film is submitted to tensile strength, which may locally induce a deviation of the Pd atomic positions from the ideal threefold fcc site, resulting in a large in-plane Pd-Pd interatomic distance distribution. This

explains why the bump in-between next Bragg peak, signature of pseudomorphic 2ML deposit, is hardly observed in the (11) CTR (see vertical lines in figure 2). Indeed, the dumping of the reflection intensity due to the Debye-Waller term is proportional to the corresponding transferred momentum q, which is larger for higher Miller indices.

In correspondence with such a large value, we cannot directly use the harmonic approximation to estimate the average displacement from the fcc site.

A more complete picture of the surface structure is obtained considering specular reflectivity too. In this case, all layers contribute to the measured signal, even if they are not in registry with the substrate. Compared to non-specular signal, it reveals the presence of two additional non-pseudomorphic partially occupied Pd layers which form before completion of the second one. Indeed, their introduction greatly improves the fit agreement factor (χ^2 decreases from 47 to 6.6,) even if their occupation rate is quite low (τ_3 = 0.28 and τ_4 = 0.09). Interplanar distances Pd_2-Pd_3 and Pd_3-Pd_4 are, within the error bar, bulk-like. Due to the small data set, both interplanar distances and Debye parameters obtained from the non-specular CTRs were kept fixed. Best fit parameter values obtained from the ensemble of CTRs are reported in table I, and the best fit curves are shown in figure 2.

Concluding, the Pd_{2ML}/Au(111) film is composed by two pseudomorphic layers, even if only the first one is complete. Before completion of the second layer, third and fourth layers start to grow. They are not in registry with the substrate, being relaxed or ill ordered parallel to the surface.

3.2 Structure of thicker adlayers

Pd_{4ML}/Au(111)

Figure 3 shows in plane H scans recorded at K=0 and L=1.05. In this reciprocal space region a diffracted signal is expected from a relaxed Pd film growing with the same crystallographic orientation of the substrate. For this thickness, an additional Pd rod at H=1.039±0.001 appears well separated from the Au CTR at H≈1. This peak is very close to the position expected for bulk Pd (H=1.048), but an in-plane strain of about 1% is still present, corresponding to an in-plane interatomic distance d_{IP}=2.776±0.003 Å (see table 2). The correlation length of Pd domains parallel to the surface is larger than 220 Å. This lower limit is found from the width of the Pd peak, which is close to the instrumental resolution.

Scanning the momentum transfer along Pd rods gives insight on the atomic stacking perpendicular to the surface. The (1.04 0) rod (figure 4) shows a first peak at about L=1.04,

which is a convolution of Pd scattering and Au background contributions. These two components can be separated at higher L values. A well-defined peak of the non-pseudomorphic Pd layer is clearly observed at L≈4.19, while the peak at L~4 comes from the Au thermal diffused scattering (TDS). This behaviour corresponds to a Pd film that grows following the underlying gold ABC stacking in the out of plane direction. Bragg peaks are in fact observed close to integer L values, following the well-known relation for fcc systems L= 3n+H-K. Pd deposit is quite rough as underlined by the absence of Kiessig fringes. More accurate values of the interlayer spacing and of the film thickness were obtained by a quantitative analysis. After standard corrections and background signal removal, deconvoluted Pd signal in the 3.5-5 L region was fitted. Pd film consists of quite high almost relaxed Pd islands. They are characterised by a well-defined interplanar distance d_{111}=2.242±0.001 Å ($d_{111(Pd\text{-}bulk)}$=2.246 Å) and their mean height is equal to 45±10 Å (20±5 ML), as obtained with the Debye-Scherrer equation. Error bars take into account for the uncertainty due to the deconvolution of the Au contribution.

For a cubic system, the value of $r = \frac{d111 \cdot \sqrt{3}}{d_{IP} \cdot \sqrt{2}}$ is equal to 1. In our case r=0.989±0.002, revealing the presence of a slight distortion with respect to the ideal cubic structure also in these relaxed islands.

Non specular CTR data analysis shows the presence of a Pd contribution in registry with the substrate that can be modeled exactly like the Pd_{2ML}/Au(111) film case. Concerning the parameters of the fitting procedure, for Pd_{4ML}/Au(111) we chose to simplify the fit, bringing out the main features of the film structure. Occupancies were of course left free, as the deposited Pd amount is different. For interlayer distances, we made the hypothesis that in the 2D (flat) region they are the same as for Pd_{2ML}: there is no reason for them to change, as they are far from islands and no additional material is deposited.

Concerning the parameters governing the signal amplitude, in the fit there is a balance in between occupancy and Debye-Waller, which have a different weight in the different rods. In particular, a decrease in the Debye-Waller improves the (11) fit but worsens the fit on the other rods. A more complex model would be required to improve the fit, as for example the introduction of layer by layer Debye-Waller, but this is submitted to hypothesis that can be hardly tested and moreover the parameters number would explode. Also, for such large Debye-Waller anharmonic terms should be considered, which is beyond our purpose. Debye Waller factors were hence kept fixed.

A summary of the structural parameters is given in table 1, while the comparison between experimental and best fit structure factors is shown in figure 5. The main difference with Pd_{2ML} is that this flat film layer does not cover the entire surface. In this case both the first and second layer occupancy were optimized, resulting in τ_{Pd1}=0.78±0.03 (instead of 1 for Pd_{2ML}/Au(111)) and in τ_{Pd2}=0.5±0.03 (instead of 0.67±0.03 for Pd_{2ML}/Au(111)), respectively.

These findings can be explained at the lightening of the previously discussed Pd rods analysis, which pointed out the growth of relaxed Pd islands. Such structures would cover a fraction of the surface inducing a loss of registry with the substrate in the underlying two first layers.

In order to validate the correspondence between loss of pseudomorphism and growth of relaxed islands, specular data analysis has been made: in this case both pseudomorphic and relaxed layers contribute to the signal. The fit has been made considering two regions with different structure and morphology. The first one ("flat deposit") corresponds to the part of the film which is mostly unaffected by the islands growth: the two first layers are pseudomorphic and may be partially covered by small clusters, as it is the case for Pd_{2ML}/Au(111). In the second region, the relaxed islands are described by truncated semi-spheres. They cover 22% of the surface, as suggested by the occupation of the pseudomorphic part of the first layer resulting from the CTR fit (τ_{Pd1}=0.78, see table 1). Occupation of the following layers follow the semi-sphere shape described imposing a diameter equal to about 220 Å corresponding to the in-plane domain size (see table 2). A few layers with lower occupancy (two in the last refinement) are allowed at the top of the islands. Thickness and top layers occupation values are obtained after minimisation of the $\chi 2$. The same Pd interplanar distance was fixed equal to the value obtained from the Pd rod analysis, d_{111}=2.242 Å. The fit gives a thickness of about 30 Å and the occupancy changes slowly with the distance from the interface due to the low height to diameter ratio (about 1/7). This thickness is in qualitative agreement with the result obtained from the Pd rods analysis, which was made on a different sample preparation with the same nominal Pd amount. For the flat part, all structural parameter values were kept fixed and equal to the non-specular CTR and to the Pd_{2ML}/Au(111) case; only adjustments of the layers occupation and of the Pd Debye were allowed.

This structural model nicely fits the experimental data (χ^2=1.6), giving a picture which is coherent with that obtained from non-specular CTR and Pd rods. We underline however that other shapes like truncated pyramids could have been used, our data not allowing to precisely state about the form of the islands. Indeed, the relaxed islands must give a sharp contribution that

is close, and hence partially hidden, to Au Bragg peaks. In our data set, islands height is deduced from the shape of reflectivity close to L=3, while far from it the signal describes the flat layer.
Summarizing, diffraction data of this sample are consistent with a Pd deposit characterized by the presence of relaxed islands, about 20±5 ML in height, covering about 20% of the surface. The remainder 80% of the film surface is flat, 2 ML thick and pseudomorphic. Its second layer is incomplete and partially covered by two atomic layers high clusters, covering about 20% of the flat region. The total equivalent Pd thickness, about 4.6 ML, is close to the nominal value.

Pd_{10ML}/Au(111)

The growth of high 3D islands is confirmed by the results obtained for a thicker deposit, Pd_{10ML}/Au(111).
As it is the case for Pd_{4ML}/Au(111), in plane measurements (figure 3) show well separated Au and Pd contributions. For the thicker film, the Pd rod position shifts towards larger H values, approaching the expected bulk position. A quantitative analysis reveals that the in-plane interatomic distance is d_{IP}=2.760±0.003 Å (see table 2). The intrinsic peak width, found using high instrumental resolution and using the Debye–Scherrer equation, gives a domain size of about 340 Å.
L scan along the (1.044, 0) Pd rod (figure 6) shows that Pd growth still follows the underlying gold ABC stacking and the absence of Kiessig fringes confirms that Pd deposit is rather rough.
Fitting of the Pd rod peak positions reveals that Pd islands relax to bulk interlayer distance. High resolution L measurements (figure 6a) show that they are about 72 ML high (Debye-Scherrer equation), hence their height grows much more quickly than their size with the deposit thickness (table 2).

3.3 Growth mechanism

Information about the first steps in the deposition process of a thin film are very important for the comprehension of the growth mechanisms. Depending on the substrate, on the deposited element and on the deposition method, different growth modes can be observed: each layer may be completed before the growing of the following one (Frank van der Merwe mode), 3D islands may be formed before the layer completion (Volmer-Weber mode) or, as an intermediate mode, 3D

islands may grow beyond a critical thickness deposited following the layer-by-layer mode (Stranski-Krastanov mode).

Figure 7 presents the *in situ* SXRD data recorded during the growth of electrochemically deposited Pd/Au(111) films in the reciprocal space anti-Bragg (0, 1, 0.5) position. Such measurements are extremely sensitive to the contribution of pseudomorphically growing Pd layers, due to the interference between substrate and overlayer scattering at the minimum of the CTR. Then, information about the growth mode can be inferred, as the anti-Bragg signal presents characteristic oscillations in correspondence of pseudomorphic layer-by-layer growth [32, 33].

These data were previously presented and discussed [18], but, due to the lack of CTR measurements, we were not able to give a detailed description of the model growth. In this frame, the structural data presented in this paper allows a deeper comprehension of the Pd electrodeposition onto Au(111).

The reflected anti-Bragg intensity undergoes a deep minimum and maximum, signature of the pseudomorphic growth of the first and second layer, respectively. In order to correctly interpret this behaviour, simulation of the anti-Bragg reflection intensity using ROD package [30] was made [18]. In correspondence of a layer-by-layer growth of the Pd film, we considered different stacking of the fcc atomic sites along the growth direction: fcc (AB sites), hcp (BC sites), or twinned fcc (BA sites). Bulk values for the Pd-Pd interlayer distance and for the Debye parameters were used, while the average of the respective bulk values was taken for the Pd-Au interlayer distance. The overall behaviour is insensitive to small variations of such values. The comparison with the experimental data undoubtedly states that, among the calculated close packed atomic structures, only the fcc pseudomorphic growth reproduces the minimum of the diffracted intensity in correspondence of the first layer completion, signature that the first Pd adlayer grows following the same fcc sequence of the substrate [18]. This feature reveals that the first layer is completed before the second one begins to be deposited. The present CTRs measurements confirm such qualitative description.

Simulation also foresees that the anti-Bragg signal increases again up to its initial intensity in correspondence with two fcc pseudomorphic layers [18]. We observe this behaviour, but the intensity reaches only about 50% of its initial value. Calculations show that this can be explained with a second layer occupancy equal to about 0.7 and the third layer starting to grow before the completion of the second one, corresponding to a non-ideal layer-by-layer growth. Meanwhile, stacking faults may induce this same behaviour and their absence needs to be confirmed.

Indeed, CTRs data presently obtained for Pd_{2ML}/Au(111) show that stacking faults contribution to the signal is negligible. CTR also quantitatively confirm that the second layer occupancy is equal to about 0.7 (see table 1, Pd_{2ML}), when third and fourth layers with relaxed lattice parameter begin to grow.

After the maximum of the anti-Brag reflected signal, the signal rapidly reaches a constant value. The film structure presently obtained with the CTRs measurements allows explaining this behaviour. It is the signature that a large amount of the deposit surface maintains the first and second layers pseudomorphic character at least up to about 10 ML as equivalent thickness. This pseudomorphic part corresponds to the region where the 3D relaxed islands do not grow.

3.4 Comparison with electrochemical characterisation

Electrochemical response may be especially sensitive to the surface structure, composition and morphology [34,35]. Nevertheless, a physical characterisation is necessary in order to validate the structural model proposed using electrochemistry.

We previously presented the electrochemical characterisation in 0.1M H2SO4 of Pd_{xML}/Pt(111)° films from 1ML up to about 10ML. Several peaks were observed. Coupling electrochemistry with *in situ* SXRD measurements in the (0,1,0.5) anti-Bragg position during Pd electrodeposition, an assignment was proposed in terms of hydrogeno(sulfate) adsorption/desorption on different layers of the deposit.

In the 0.25 - 0.35 V_{RHE} potential region, a bump and a sharp peak (0.284/0.286 V_{RHE}) were attributed to adsorption/desorption processes onto the first pseudomorphic layer [36]. A peak at 0.275/0.281 VRHE was assigned to the response of second pseudomorphic plane.

Present *in situ* SXRD analysis, confirming the incomplete layer-by-layer pseudomorphic growth of the two first layers, is in complete agreement with the presence of different electrochemical responses for the adsorption/desorption processes on each of the two first Pd layers. It also confirms quantitative results given with electrochemistry on the layers occupation. Charge analysis suggested that a small area of the first Pd layer remains free up to 4ML (30% of the first Pd layer uncovered for Pd_{2ML}/Au(111) and 10% for Pd_{4ML}/Au(111)): such values are in particularly good agreement with SXRD results (30% and 20%, respectively).

Beyond the two first Pd layers, the electrochemical peak at 0.261/0.264 V_{RHE} was relied to adsorption/desorption on the third and following relaxed planes. Relying on the fractal and rough growth previously related by Kibler et al. using STM [12], specific charge behaviour under the

peaks as a function of the thickness was interpreted as due to the presence of vertically growing 3D islands. Their footprint on the surface seemed to represent only a small fraction of the electrode's surface and the free surface of the second layer appeared not to significantly evolve, at least up to about 10ML. Present *in situ* SXRD data agree with this description, pointing out the presence of thick 3D Pd like relaxed islands appearing beyond 2ML. Compared to STM, our data give a statistical average of this morphology over a macroscopic region of the sample surface. They grow vertically, occupying only about 22% of the Pd4ML/Au(111)° film surface (see table 2), and their height grows more rapidly than their lateral size while thickness increases from 4ML to 10ML.

Finally, *in situ* SXRD data presented in this paper unequivocally correlate the features observed during the electrochemical surface characterisation in acidic medium with the detailed structure of the Pd film, definitely establishing the use of electrochemistry for surface characterisation of this system.

4. Conclusion

We have characterized the structure of ultra-thin Pd films electrochemically deposited onto Au(111) single crystal in a chloride containing solution. *In situ* Surface X-Ray Diffraction allows the detailed description of the deposition growth mode, as well as the film morphology and the lattice parameters as a function of the thickness, from 2 ML up to 10 ML as equivalent thickness.

The growth mode was studied measuring in real time the intensity variations of an anti-Bragg reflection. This experiment can be interpreted with a non-ideal layer-by-layer pseudomorphic growth up to two monolayers. The third layer formation starts before the completion of the second one. This growth mode was clearly confirmed by the quantitative analysis of the CTRs. Pd_{2ML}/Au(111) film is quite smooth. It is described by two pseudomorphic layers, but the occupation of the second plan is equal to about 0.7. On top of the second layer islands one or two atomic layers high are found that cover about 20% of the surface. They are not in registry with the surface.

For higher thickness, high 3D relaxed islands begin to grow. For Pd_{4ML}/Au(111) the experimental data are well described by 3D islands about 20±5 ML high and ~220 Å as diameter. They occupy about 20% of the total surface, while the remaining surface is covered by flat pseudomorphic Pd film with the same structure as Pd_{2ML}/Au(111).

With thickness increasing, islands continue to grow and their height increases much faster than their size: for Pd_{10ML}/Au(111) they are about 72 ML high and 340 Å as a diameter.

The present SXRD study confirms that electrochemical characterization of the Pd/Au(111) surface made in sulphate solution is correct, reliable and extremely sensitive. It gives information not only on the surface structure of the electrode, discriminating between first, second and following bulk like layers organized as 3D huge islands, but also to possible electronic effects due to the underlying deposit, being able to distinguish between the first (Au underlying) and the second (Pd underlying) pseudomorphic Pd planes.

We could also clearly show that chloride do not play any role in inhibiting the three dimensional growth of Pd films electrodeposited onto Au(111). Pd deposit rapidly becomes quite rough, with huge Pd bulk like islands vertically growing on about 20% of the surface. This behaviour is quite different compared to Pd electrodeposition onto Pt(111). In a previous paper, we discussed the important role that chloride has in favouring the layer-by-layer growth in this last case [37]. We showed that the pseudomorphic character of the Pd film deposited onto Pt(111)° in chloride containing solution preserved over about 10 fully occupied layers. The present results show that anions may have a strong influence on the deposit structure not only of the very first layers, but also beyond, and it strongly depends on both deposited metal and substrate chemical nature.

Acknowledgements

Beamtime is acknowledged at the French D2AM beamline of the ESRF. We are grateful to the beamline staff for its technical support in making the SXRD measurements. PhD work of Liang Wang was founded by China Scholarship Council (CSC).

References

[1] A. Wieckowski, Interfacial electrochemistry, Marcel Dekker Inc., New York, Basel, 1999.

[2] P.Allongue and F. Maroun *Current Opinion in Solid State and Material Science* 2006 **10** 173.

[3] M. Baldauf, D.M. Kolb *J. Phys. Chem.* 1996 **100** 11375.

[4] H. Naohara, S. Yen and K. Uosaki *J. Electroanal. Chem*. 2001 **500** 435.

[5] T.J. Schmidt, V. Stamenkovic, N.M. Markovic, P.N. Ross *Electrochim. Acta* 2003 **48** 3823.

[6] A.M. El-Aziz, L.A. Kibler *J. Electroanal. Chem.* 2002 **534** 107.

[7] H. Naohara, S. Yen and K. Uosaki *Electrochim. Acta* 2000 **45** 3305.

[8] M. Baldauf, D.M. Kolb *Electrochim. Acta* 1993 **38** 2145.

[9] H. Duncan, A. Lasia *Electrochim. Acta* 2007 **52** 6195.

[10] J. Tang, M. Petri, L.A. Kibler, D.M. Kolb *Electrochim. Acta* 2005 **51** 125.

[11] C. Köntje, L.A. Kibler, D.M. Kolb *Electrochimica Acta* 2009 **54** 3830.

[12] L.A. Kibler, M. Kleinert, R. Randler, D.M. Kolb *Surf. Science* 1999 **443** 19.

[13] M. Takahasi, Y. Hayashi, J.-I. Mizuki, K. Tamura, T. Kondo, H. Naohara, K. Uosaki *Surf. Science* 2000 **461** 213.

[14] B.E. Koel *Phys. Rev. B* 1999 **46** 7846.

[15] H. Naohara, S. Hen, K. Uosaki *J. Phys. Chem. B* 1998 **102** 4366.

[16] H. Naohara, S. Hen, K. Uosaki *Colloids and Surface A: Physicochemical and engineering aspects* 1999 **154** 201.

[17] M. Takahasi, K. Tamura, J. Mizuki, T. Kondo, K. Uosaki *J. Phys.: Condens. Matter* 2010 **22** 474002.

[18] E. Sibert, L. Wang, M. De Santis, Y. Soldo-Olivier *Electrochim. Acta* 2014 **135** 594.

[19] D.M. Kolb *Progress in Surf. Science* 1996 **51** 109.

[20] J. V Barth., H. Brune, G. Ertl *Phys. Rev. B* 1990 **42** 9307.

[21] H. Bulou and C. Goyhenex *Phys. Rev. B* 2002 **65** 45407.

[22] O. M. Magnussen, K. Krug, A. H. Ayyad, J. Stettner *Electrochim. Acta* 2008 **53** 3449.

[23] M. S. Zei, G. Lehmpfuhl, D. M. Kolb *Surf. Sci.* 1989 **221** 23.

[24] K. P. Bohnen, D. M. Kolb *Surf. Sci.* 1998 **407** L629.

[25] C. Lebouin, Y. Soldo-Olivier, E. Sibert, M. De Santis, F. Maillard, R. Faure *Langmuir* 2009 **25 (8)** 4251.

[26] Y. Soldo, E. Sibert, G. Tourillon, J.L. Hazemann, J.-P. Levy, D. Aberdam, R. Faure, R. Durand *Electrochimica Acta* 2002 **47** 3081.

[27] I.K. Robinson *Phys. Rev. B* 1986 **33** 3830.

[28] E. Vlieg, *J. Appl. Crystallogr*. 1997 **30** 532.

[29] I. K. Robinson Handbook on Synchrotron Radiation; North-Holland: Amsterdam, 1991, Brown, G.S., Moncton, D. E. Eds.; Vol. 3, p 221.

[30] E. Vlieg, *J. Appl. Crystallogr*. 2000 **33** 401.

[31] E. Lundgren, B. Stanka, M. Schmid and P. Varga *Phys. Rev. B* 2000 **62** 2843.

[32] K. Krug, J. Styettner, O. Magnussen *Phys. Rev. Lett*. 2006 **96** 246101.

[33] E. Weschke, C. Schüßler-Langeheine, R. Meier, G. Kaindl, C. Sutter, D. Abernathy, G. Grübel *Phys. Rev. Lett.* 1997 **79** 3954.

[34] L.A. Kibler, Á. Cuesta, M. Kleinert, D.M. Kolb, J. Electroanal. Chem. 2000 **484** 73

[35] C. Lebouin, Y. Soldo-Olivier, E. Sibert, P. Millet, M. Maret, R. Faure *J. Electroanal. Chem*. 2009 **626** 59.

[36] E. Sibert, L. Wang, M. De Santis, Y. Soldo-Olivier, *Electrochim. Acta* 2014 **135** 594.

[37] Y. Soldo-Olivier, M. C. Lafouresse, M. De Santis, C. Lebouin, M. de Boissieu, E. Sibert, *J. Phys. Chem. C* 2011 **115(24)** 12041.

Figures

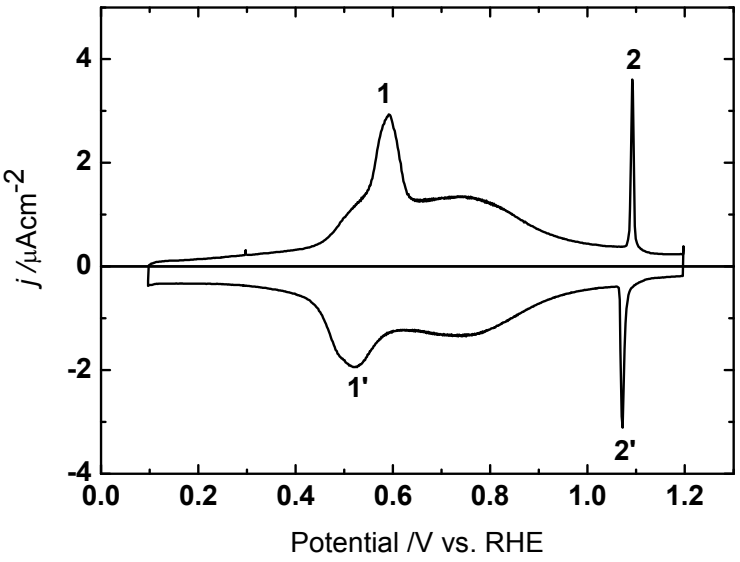

Figure 1: Cyclic voltammogram of Au(111) in 0.1 M H_2SO_4 solution, scan rate 10 mVs^{-1}.

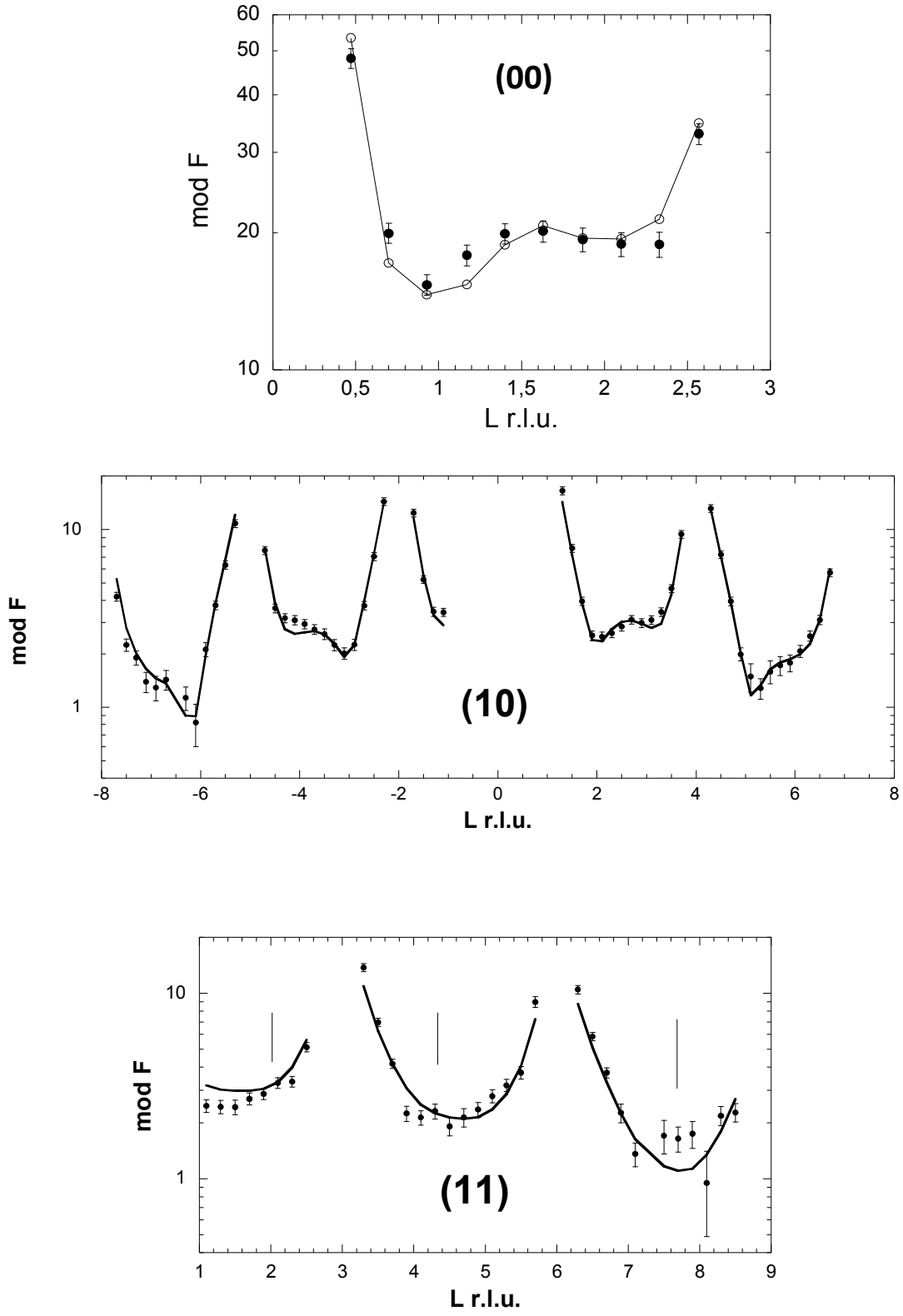

Figure 2: Pd_{2ML}/Au(111): specular (00); non-specular (10) and (11) CTRs; experimental data (black circles) with error bars and fitting (continuous line). Vertical lines in (11) CTR indicate the bumps between the Bragg peaks.

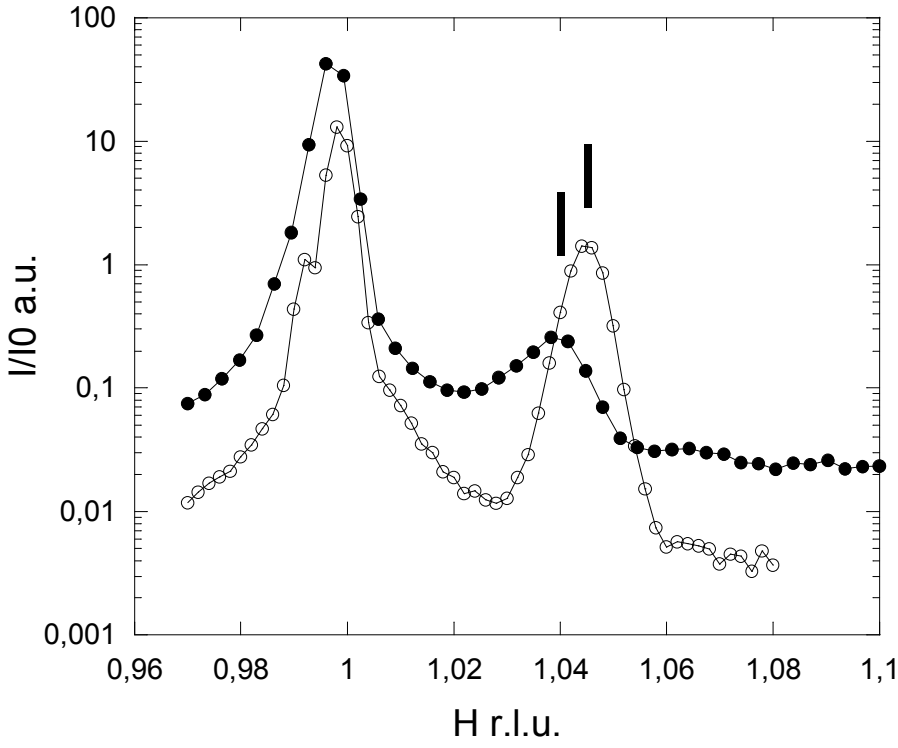

Figure 3: H scans measured for Pd_{4ML}/Au(111) at K=0, L=1.05 (black circles) and for Pd_{10ML}/Au(111) at K=0, L=1.046 (empty circles). For the 10 ML scan the slit width is reduced to improve instrumental resolution. Vertical lines indicate the peaks position.

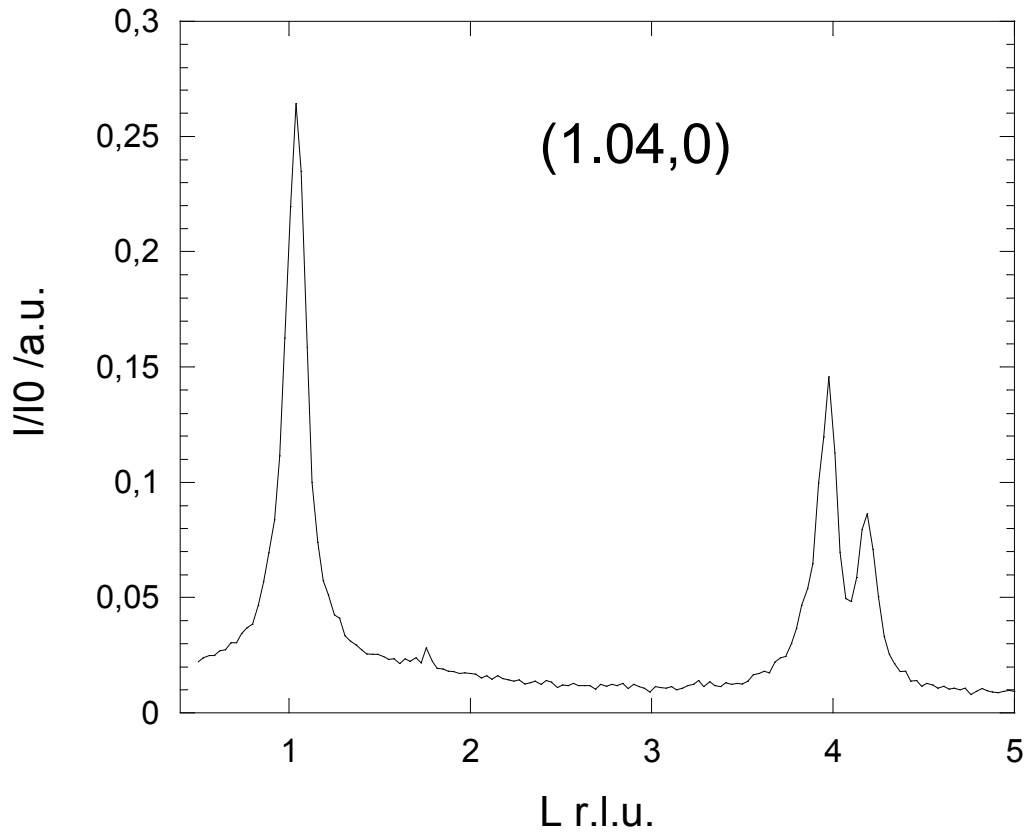

Figure 4: Pd_{4ML}/Au(111): L scan at H=1.04, K=0**.**

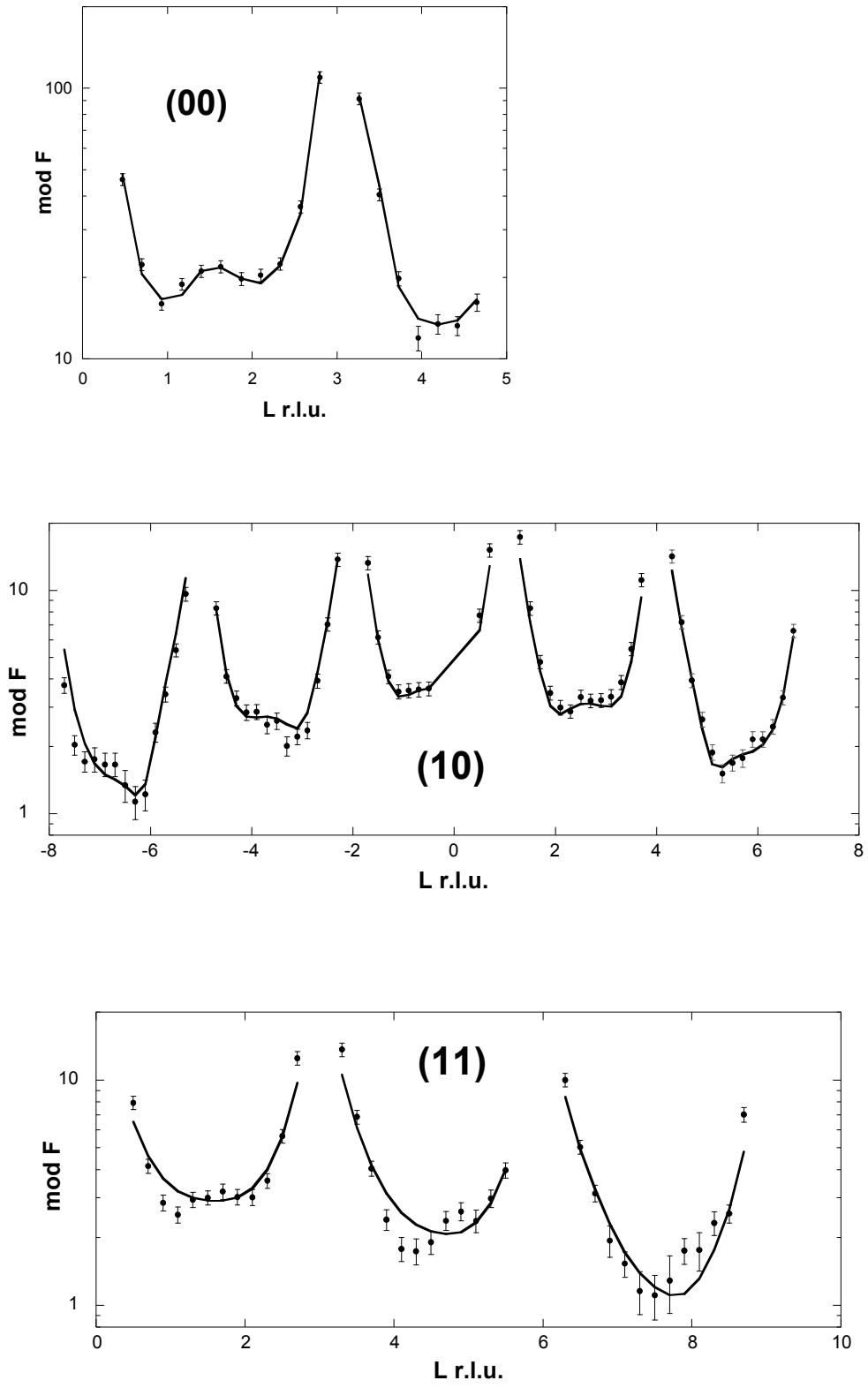

Figure 5 : Pd_{4ML}/Au(111): a) specular (00); b), c) non-specular (10) and (11) CTRs.

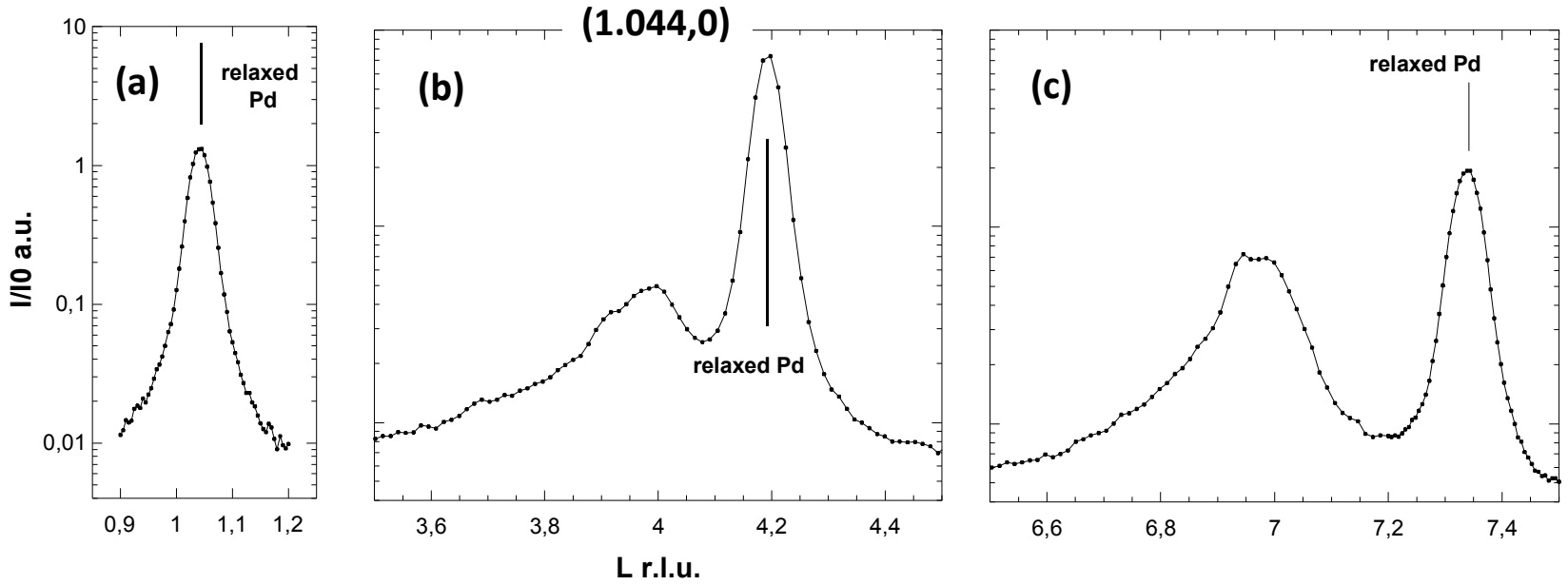

Figure 6. Pd_{10ML}/Au(111):L scans a), b), c) in different intervals along the (1.044 0) rod. (6a) is performed with a high resolution of the momentum transfer perpendicular to the surface. Vertical lines indicate the relaxed Pd contribution.

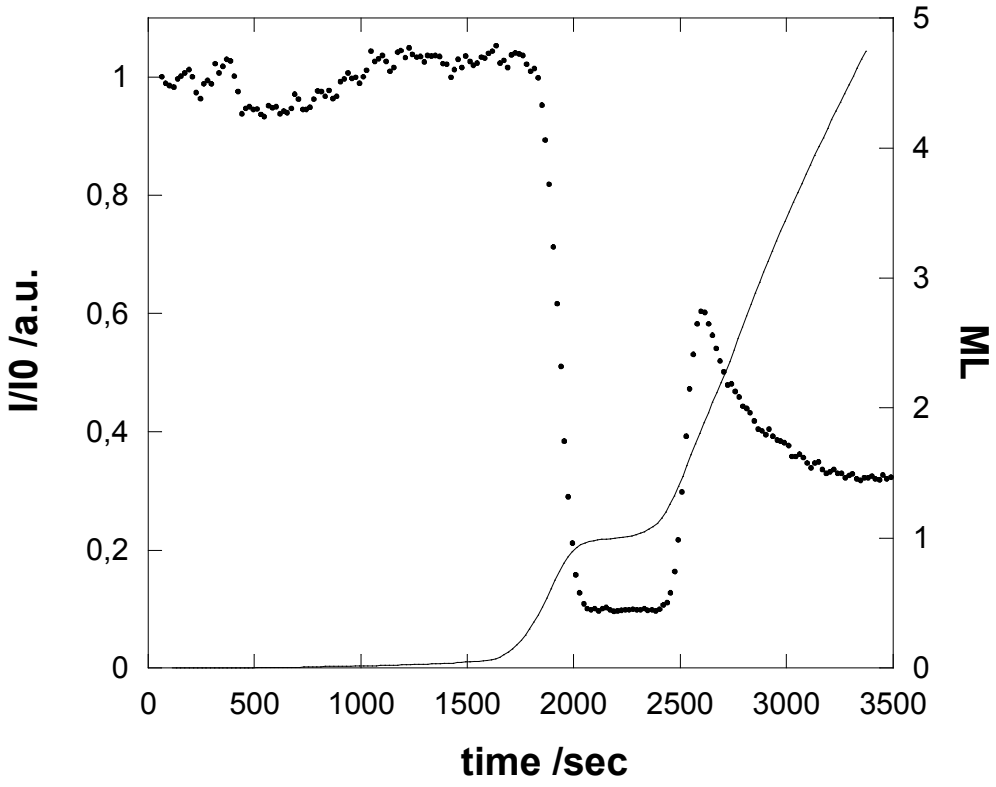

Figure 7: Au(111) in 10^{-4} M $PdCl_2$ + $3 \cdot 10^{-3}$ M HCl + 0.1 M H_2SO_4. Pd equivalent coverage (continous line) and normalized diffracted signal at (0, 1, 0.5) (dotted line). Counting time for each recorded point in SXRD experiment is 18 seconds. Potential was scanned from 1 V *vs.* RHE (t=0 s) down to 0.718 V *vs.* RHE (t=2700 s) at 0.1 mV s^{-1} and then hold at 0.718 V *vs.* RHE.

Tables

Table 1 : Best fit values obtained from the non-specular and specular CTRs. DW is the Debye-Waller parameter**.**

	Pd_{2ML}/Au(111)		Pd_{4ML}/Au(111)		
	non specular	**specular**	**non specular**	**Specular**	
				"flat" deposit	***3D islands***
τ_{Pd1}	1*	1*	0.78±0.03	0.78*	$1 \le N \le 13$ τ_{PdN}≈0.22 τ_{Pd14}=0.06±0.03 τ_{Pd15}=0.06±0.03
τ_{Pd2}	0.67±0.03	0.71±0.02	0.50±0.03	0.58±0.05	
τ_{Pd3}	-	0.28±0.02	-	0.23±0.02	
τ_{Pd4}	-	0.09±0.01	-	0.10±0.01	
$\tau_{Pd(N>4)}$	-	-	-	-	
d_{Au-Au}	2.328±0.004 Å	2.328 Å*	2.328 Å*	2.328 Å*	2.328 Å*
d_{Au-Pd1}	2.275±0.015 Å	2.275 Å*	2.275 Å*	2.275 Å*	2.275 Å *
$d_{Pd1-Pd2}$	2.20±0.03 Å	2.20 Å*	2.20 Å*	2.20 Å*	2.242 Å#
$d_{Pd2-Pd3}$	-	2.28±0.05Å		2.28 Å*	
$d_{Pd3-Pd4}$	-	2.2±0.1Å		2.2 Å*	
$d_{PdN-Pd(N-1)}$ $N\geq5$	-	-	-	-	
Au DW	0.8 $Å^2$*	0.8 $Å^2$*	0.8$Å^2$*	0.8 $Å^2$ *	
Au last layer DW	1.27±0.06 $Å^2$	1.27 $Å^2$*	1.27$Å^2$*	1.27 $Å^2$*	
Out of plane Pd DW	0.44±0.25 $Å^2$	0.44 $Å^2$*	0.44 $Å^2$ *	4±2$Å^2$	0.44 $Å^2$*
In plane Pd DW	15±1 $Å^2$	-	15 $Å^2$*	-	-
χ^2	3	6.6§	3	1.6	

* fixed parameters
# value obtained from L scan, see figure 6
§ such high value of χ^2 is due to the small number of measured point (10) and relatively high number of extracted parameters (5)

Table 2 : Structural parameters obtained from the in-plane (H scan) and out-of-plane (L scan) measurements across and along Pd rods.

In plane			
	Interatomic distance	Domain size	$\frac{d_{film} - d_{bulkPd}}{d_{bulkPd}}$
Pd_{4ML}/Au(111)	2.776±0.003 Å	> 220 Å	0. 9±0.1%
Pd_{10ML}/Au(111)	2.760±0.003 Å	~ 340 Å	0. 3±0.1%

Out of plane			
	Interplanar distance	Height	$\frac{d_{film} - d_{bulkPd}}{d_{bulkPd}}$
Pd_{4ML}/Au(111)	2.242±0.002 Å	45±10 Å	-0. 2±0.1%
Pd_{10ML}/Au(111)	2.249±0.002 Å	~ 162 Å	0. 1±0.1%.